Journal of Colloid and Interface Science 605 (2022) 582–591

Contents lists available at ScienceDirect

Journal of Colloid and Interface Science

journal homepage: www.elsevier.com/locate/jcis

On-demand transdermal insulin delivery system for type 1 diabetes therapy with no hypoglycemia risks

Yun Fu [a,1], Peng Liu [b,1], Meng Chen [a], Tongxia Jin [a], Huijing Wu [a], Mingyang Hei [a], Congrong Wang [c,*], Yufang Xu [a], Xuhong Qian [a], Weiping Zhu [a,*]

[a] State Key Laboratory of Bioreactor Engineering, Shanghai Key Laboratory of Chemical Biology, School of Pharmacy, East China University of Science and Technology, 130 Meilong Road, Shanghai 200237, China
[b] Shanghai Jiao Tong University Affiliated Sixth People's Hospital, Shanghai Key Laboratory of Diabetes, 600 Yishan Road, Shanghai 200233, China
[c] Department of Endocrinology & Metabolism, Shanghai Fourth People's Hospital, School of Medicine, Tongji University, Shanghai 200434, China

GRAPHICAL ABSTRACT

A dissolving microneedle patch (SGRM patch) containing mesoporous silica nanoparticles (G-MSN@Insulin@ZnO-PBA-2) was developed for transdermal delivery of insulin. A glucose-dependent release manner was achieved due to the sensitive Wulff-type glucose responsive linker. The *in vivo* results suggested that the systems displayed excellent glycemic control and avoided the risks of hypoglycemia, which could result in the development of desirable smart insulin delivery system with the potential for clinical application.

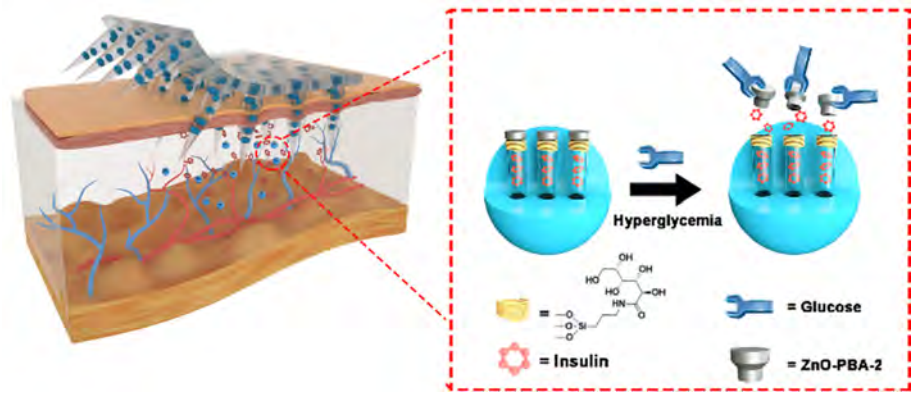

ARTICLE INFO

Article history:
Received 26 March 2021
Revised 20 July 2021
Accepted 25 July 2021
Available online 28 July 2021

Keywords:
Controlled insulin delivery
Glucose responsive

ABSTRACT

Diabetes is a metabolic disease that is affecting an ever-increasing number of people worldwide, resulting in increased burdens on healthcare systems and societies. Constant monitoring of blood glucose levels is required to prevent serious or even deadly complications. One major challenge of diabetes management is the simple and timely administration of insulin to facilitate consistent blood glucose regulation and reduce the incidence of hypoglycemia. With this research, we construct an insulin delivery system, the delivery system is comprised of phenylboronic acid based fluorescent probes, which is used as glucose responsive linkers, mesoporous silica nanoparticles providing an insulin reservoir, and zinc oxide nanoparticles used as gate keepers. The system with glucose sensitive responsive linker exhibits controlled release of insulin under high glucose concentrations, providing prolonged blood glucose

* Corresponding authors.
E-mail addresses: crwang@tongji.edu.cn (C. Wang), wpzhu@ecust.edu.cn (W. Zhu).
[1] These authors contributed equally.

https://doi.org/10.1016/j.jcis.2021.07.126

Phenylboronic acid
Microneedle patch

regulation and no risks of hypoglycemia. Furthermore, the system is combined with a hyaluronic-acid based microneedle patch, which exhibit efficient skin penetration for transdermal delivery. With our system, the nanoparticles provide outstanding *in vivo* glucose regulation when administrated by subcutaneous injection or via transdermal microneedle patch. We anticipate that our biocompatible smart glucose responsive microneedle patch (SGRM patch) will facilitate the development of clinically useful systems.

1. Introduction

Diabetes mellitus is a chronic metabolic disorder characterized by high blood glucose levels (BGLs), and is caused by insufficient insulin supply or insulin resistance, and currently affects millions of people worldwide [1,2]. Importantly, the number of diabetic patients worldwide is expected to soar from 425 million in 2019 to 700 million by 2045 [3]. People with diabetes have a higher risk of developing life-threatening complications, including cardiovascular disorders, renal diseases, foot infectious, and can even lead to amputation [4–7]. However, postprandial injection of insulin using a syringe is painful and inconvenient for patients with type 1 diabetes and advanced type 2 diabetes, which leads to poor treatment compliance. In addition, costly insulin pumps need periodic replacement, which may increase the risk of infection [8].

In order to address these problems, various synthetic close-looped insulin delivery systems have been developed to regulate the BGLs [9], which are based on different glucose-responsive moieties, such as glucose oxidase (GOx) [10,11], glucose-binding proteins (e.g., Concanavalin A) [12,13] and phenylboronic acids (PBAs) [14,15]. Glucose oxidase is a glucose-specific protein, which catalyzes the oxidation of glucose to generate gluconic acid and hydrogen peroxide. The altered microenvironment (such as local pH [16], H_2O_2 concentration [17], and O_2 level [18]) during this period triggered the disassembly of the nanoparticles to release the loaded insulin [19–22]. Concanavalin A is a lectin, capable of binding to saccharides, which has been grafted to polymer chains in order to construct nano-systems [23,24].

PBAs are of low toxicity, stable and are easy to modify. Importantly, PBAs form reversible dynamic covalent bonds with the *cis*-1,2-diols and *cis*-1,3-diols of saccharides [25–27]. Therefore, some PBAs-based glucose-responsive drug delivery systems have been reported [28–30]. However previous researches have demonstrated that PBAs with lower pKa display higher affinity towards carbohydrates at neutral pH, which makes unmodified PBA (pKa $\approx 8 \sim 9$) unsuitable for clinical use [31]. One way to address this problem is to introduce electron-withdrawing groups to the benzene ring [32,33]. For example, Yasuhisa et.al have developed a gel containing fluorine modified PBAs that swells in response to glucose under physiological conditions [34]. On the other hand, the combination of PBAs and glycosyl units favors the formation of stable and soluble phenylboronic ester, thus decreases the pKa of the PBAs and increases their sensitivity towards glucose under physiological conditions [35,36]. By introducing glucosamine into the polymer, Shi et.al have developed nanoparticles that can release insulin at pH = 7.4 with better glucose sensitivity due to the lowered pKa of PBAs [37]. In addition the intramolecular interaction between B and N atoms in Wulff-type boronic acids can lower the pKa of PBAs, which stabilizes the formation of boronate esters at physiological pH [38]. In fact, the detection limit of some Wulff-type fluorescent probes for D-glucose is at the millimolar level, which is the same order of magnitude concentration of glucose as that found in human blood, making PBAs based fluorescent probes promising candidates for responding to changes in biologically relevant glucose levels [39]. Inspired by these works, we believe that some Wulff-type fluorescent probes for glucose could be used as glucose-responsive moieties to construct the close-looped insulin delivery systems.

Here, we report on a 'smart' insulin delivery system directly utilizing glucose-sensitive fluorescent probe as the responsive moiety. As shown in Scheme 1, we chose mesoporous silica nanoparticles (MSNs) as the insulin reservoir due to their stability, significant loading capacity and biocompatibility [40]. The anthracene-based monoboronic acid 3 [41], a glucose probe, was firstly used as a sensitive 'linker' (PBA-2) to regulate the insulin release at high BGLs. The PBA-2 grafted zinc oxide dots (ZnO-PBA-2) were used as the 'gate keepers' to block insulin's escaping from the MSNs at normal BGLs. However, at high BGLs, the connection between PBA-2 and gluconamide attached to the MSN was cleaved to facilitate the release of insulin. In order reduce the pain of injection and improve patient compliance, a dissolving microneedle patch was prepared to load this nano-system, resulting in a system that was minimally invasive, easy to use and did not require specialized training to operate [42–45]. The hyaluronic-acid based microneedle patch displayed significant mechanical strength and appropriate needle length for puncturing the dermis. Therefore, we utilized these microneedle patches loaded with smart glucose responsive PBAs based mesoporous silica nanoparticles to develop a suitable system for the transdermal delivery of insulin (smart glucose responsive microneedle patch, SGRM patch). We observed that the system displayed excellent glycemic control, avoided hypoglycemia, and could result in the development of desirable smart insulin delivery system with the potential for clinical application.

2. Materials and methods

2.1. Materials

Hexadecyl trimethylammonium bromide (CTAB, 98%) and lithium bromide (99.995%) were purchased from Sinopharm Chemical Reagent Co., Ltd. (Shanghai, China). Ethyl orthosilicate (TEOS, AR), *n*-hexane (AR), aqueous ammonia (25%-28%), potassium hydroxide (AR) and anhydrous ethanol (AR) were purchased from Shanghai Lingfeng chemical reagent Co., Ltd. (Shanghai, China). Zinc acetate dihydrate (99%) and monomethylamine solution (25%-30%) were purchased from Titan Scientific co., Ltd. (Shanghai, China). 4-aminobenzoic acid (99%), m-toluidine (98%), anthraquinone (98%), 1-(3-dimethylaminopropyl)-3-ethylcarbodii mide hydrochloride (EDCI, 99%), *N*-hydroxysuccinimide (NHS, 98%), N-(3-triethoxysilylpropyl)gluconamide (50% in ethanol), and D-(+)-glucose (99%) were purchased from J&K Scientific Co., Ltd. (Beijing, China). 2-formylbenzeneboronic acid (97%), sodium borohydride (98%), sodium hydride (60%), trimethylsulfonium iodine (98%), (3-aminopropyl) triethoxysilane (APTES, 98%), (3-iso cyanatopropyl)triethoxysilane (95%), fluorescein-5-isothiocyanate (FITC, 97%) were purchased from Energy Chemical Technology Co., Ltd. (Shanghai, China). Porcine insulin (98.8%) was purchased from Xuzhou Wanbang Jinqiao pharmaceutical Co., Ltd. (Jiangsu, China). Streptozotocin (STZ, 98%) was bought from Sigma-Aldrich

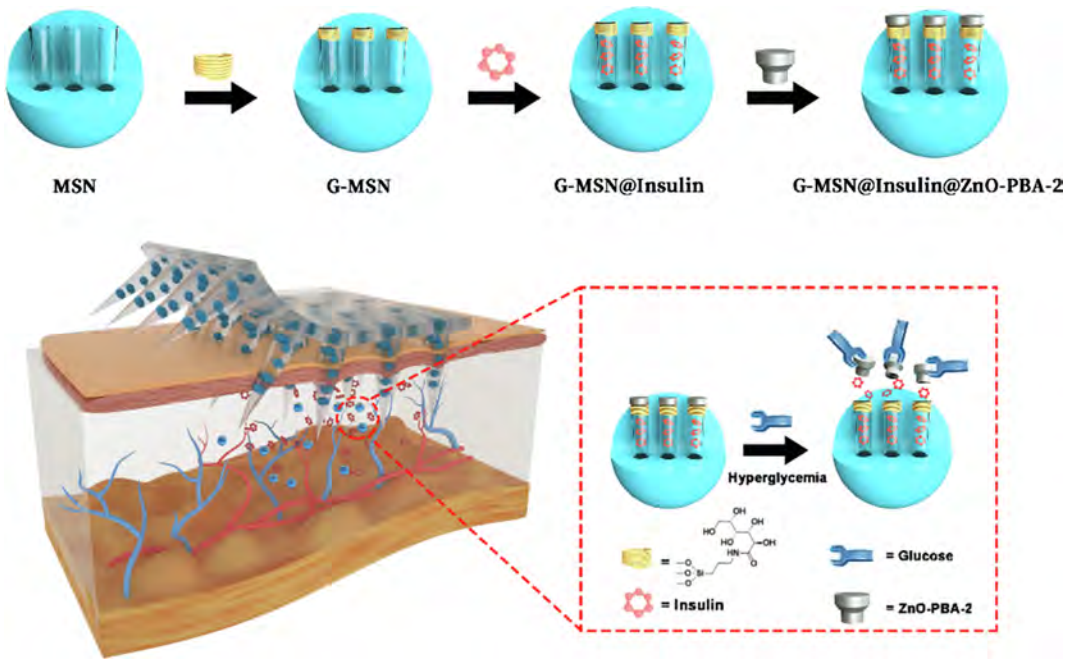

Scheme 1. Schematic illustration of preparation of SGRM patch containing G-MSN@Insulin@ZnO-PBA-2 and its anti-diabetic mechanism after treated on skin. (The top line: preparation of G-MSN@Insulin@ZnO-PBA-2; The bottom line: anti-diabetes mechanism of SGRM patch.

(Shanghai, China). The phosphate buffer saline (PBS) was purchased from Tianjin Haoyang Biological Manufacture Co., Ltd. (Tianjin, China).

2.2. Preparation of G-MSN

First, 1.0 g CTAB was evenly dispersed in 160.0 mL deionized water, then 5.0 mL aqueous ammonia was added. The mixture was magnetically stirred at 35.0 °C to form a clear solution. After that, the mixture of 20.0 mL *n*-hexane and 5.0 mL tetraethyl orthosilicate was added dropwise to the solution in 30 min. The reaction was continued for 12 h. After that, the resulting product was filtered, washed and dried to obtain MSN.

Then, 1.0 g MSN was evenly dispersed in 100.0 mL ethanol. 1.0 mL N-(3-triethoxysilylpropyl)gluconamide was added, and the reaction was stirred for 15 h at room temperature under argon. The product was filtered, washed and then dried to obtain G-MSN^0.

Finally, 200.0 mg G-MSN^0 was evenly dispersed in 47.5 mL ethanol. Then 500.0 mg ammonium nitrate dissolved in 2.5 mL water was added. The reaction was heated to reflux for 24 h. The product was filtered, washed, and dried to obtain G-MSN.

2.3. Preparation of FITC-Insulin

FITC labeled insulin was synthesized to conduct the related experiments such as confocal microscopy of the SGRM patch and the *in vitro* release profile of the nanoparticles.

Briefly, 200.0 mg insulin was dissolved in 50.0 mL 0.1 M Na_2CO_3 buffer (pH = 9.0), then 2.5 mg FITC in 2.5 mL DMSO was added dropwise to the insulin solution. After stirring for 2 h at room temperature in the dark, the reaction solution was transferred to a dialysis bag (MWCO = 1000 D) and dialyzed for 48 h, and the dialysate was changed every 6 h. Finally, 188.0 mg yellow solid, FITC-Insulin, was obtained by lyophilization and refrigerated before further use.

2.4. Preparation of ZnO-PBA-1 and ZnO-PBA-2

Two PBA linkers PBA-1 and PBA-2 were synthesized according to the literature methods (Fig. S1, Fig. S2) [41,46].

ZnO and ZnO-NH_2 were synthesized according to the literature with moderate improvement [47]. For ZnO dots, 3.95 g zinc acetate dihydrate and 100 mL ethanol were added into a 500 mL three-necked flask and heated to 70 ℃ under mechanical agitation. After the reaction solution was clear and transparent, 2.10 g KOH was dissolved in 90 mL ethanol and added to the above system in 30 min. Then the mechanical stirring was continued (600 rpm). The reaction was maintained at 70 ℃ for 3 h. ZnO dots were obtained by centrifugation and washed with ethanol several times and finally freeze-dried to obtain 1.2 g white solid.

For ZnO-NH_2 dots, 3.95 g zinc acetate dihydrate and 100 mL ethanol were added into a 500 mL three-necked flask and heated to 70 ℃ under mechanical agitation. After the reaction solution was clear and transparent, 2.10 g KOH was dissolved in 90 mL ethanol and added to the above system in 30 min. Then the mechanical stirring was continued (600 rpm). The reaction was maintained at 70 ℃ for 3 h. After that, 5 mL APTES was added to the above system, and mechanical stirring was continued for 1 h. After 1 h, ZnO-NH_2 dots were obtained by centrifugation and washed with ethanol several times and finally freeze-dried to obtain 1.4 g white solid.

ZnO-PBA-1 was synthesized as follows (Fig. S3). Firstly, a 50.0 mL two-neck round bottom flask was added with 12.3 mg PBA-1, 7.4 mg EDCI, 4.4 mg NHS, and 30.0 mL of ultrapure water, then the pH was adjusted to 7.0. The reaction was stirred at room temperature for 4 h. Then 300.0 mg of ZnO-NH_2 was added to the above system and stirred for 4 h at room temperature. After 4 h, the reaction was centrifuged, washed, and lyophilized to obtain 280.0 mg of ZnO-PBA-1 as red solid.

ZnO-PBA-2 was synthesized as follows (Fig. S4). Firstly, a 50.0 mL two-neck round bottom flask was added with 12.2 mg PBA-2, 15.7 mg (3-isocyanatopropyl)triethoxysilane, 0.15 mL triethylamine and 10.0 mL anhydrous tetrahydrofuran. The reaction was heated at reflux under argon for 24 h. After 24 h, the solvent

was evaporated. Then 300.0 mg ZnO and 40.0 mL anhydrous DMF were added. The mixture was then heated to 120 °C for 30 min. Finally, the mixture was centrifuged, washed, and lyophilized to obtain 274.0 mg of ZnO-PBA-2 as yellow solid.

2.5. Preparation of the G-MSN@Insulin@ZnO-PBA-1 and G-MSN@Insulin@ZnO-PBA-2

G-MSN@Insulin@ZnO-PBA-1 was prepared as follows. 10.0 mg G-MSN and 5.0 mg insulin were added to 4.0 mL HCl solution (pH = 2.0). The mixture was then stirred at room temperature for 24 h and centrifuged to remove the supernatant. Then 15.0 mg of ZnO-PBA-1 in 3.0 mL of PBS buffer (pH = 7.4) was added to the mixture of G-MSN@Insulin and stirred at room temperature for 24 h. The reaction was then centrifuged, washed and lyophilized to obtain G-MSN@Insulin@ZnO-PBA-1 as white solid.

G-MSN@Insulin@ZnO-PBA-2, G-MSN@FITC-Insulin@ZnO-PBA-1, and G-MSN@FITC-Insulin@ZnO-PBA-2 were prepared similarly.

2.6. In vitro glucose response measurements

The *in vitro* glucose response measurements of G-MSN@FITC-Insulin@ZnO-PBA-1 and G-MSN@FITC-Insulin@ZnO-PBA-2 were evaluated by adding these nanoparticles to different concentration of glucose solutions (0 mg/dL, 180 mg/dL, 450 mg/dL, 900 mg/dL). Then, at specific times, 0.5 mL samples were taken from the solution and centrifuged. 0.1 mL of the upper solution was added to a cuvette and the fluorescent intensity of FITC-Insulin at 488 nm was measured using a fluorescence spectrophotometer. To access the responsiveness of G-MSN@FITC-Insulin@ZnO-PBA-2, the nanoparticles were incubated under glucose concentration increasing from 180, 450 to 900 mg/dL every 1 h. And G-MSN@FITC-Insulin@ZnO-PBA-2 were also incubated under glucose concentration between 0 and 180 mg/dL every 2 h.

2.7. Experimental animals

All rats and mice were purchased from Shanghai SLAC Laboratory Animal Co., Ltd. and grouped in clean dry cages at 25 ± 1 °C under a 12 h light 12 h dark automatic lightening with food and water ad libitum. All the experiments complied with the National Institutes of Health Guide for the Care and Use of Laboratory Animals in Shanghai, China. All the experiments were performed with the permission of the Ethics Committee on Laboratory Animal Care of Shanghai Jiao Tong University Affiliated Sixth People's Hospital.

2.8. In vivo studies on rats

Type 1 diabetic rat models were induced according to the protocol [48]. STZ was dissolved in sodium citrate buffer (pH = 4.5) (0.01 g/mL). STZ dosage was set at 75.0 mg/kg for rats. After 3 weeks, any fasted rat that has a BGLs > 16.7 mmol/L was regarded as the stable type 1 diabetes model. The BGLs were tested by monitoring tail vein blood samples with a glucose meter (Roche, ACCU-CHEK).

The established type 1 diabetic rats were divided into 3 groups and subcutaneously injected with different samples, including PBS, G-MSN@Insulin@ZnO-PBA-2 (20.5 IU/kg) and insulin (20.5 IU/kg). The fasting BGLs were tested over time until they returned to high levels.

Intraperitoneal glucose tolerance tests (IPGTTs) were conducted to evaluate the *in vivo* therapeutic effects of G-MSN@Insulin@ZnO-PBA-2. Briefly, diabetic rats were divided into 2 groups and subcutaneously injected with G-MSN@Insulin@ZnO-PBA-2 (20.5 IU/kg) and insulin (20.5 IU/kg) respectively. Healthy rats were used as control. After 2.5 h, rats were intraperitoneally injected with glucose solution (1.5 g/kg). BGLs were measured by tail blood samples every 15 min for 2 h. The glucose area under the curve (AUC) between 0 and 120 min was adopted to assess the responsiveness of the nanoparticles towards blood glucose, in comparison with the other groups.

Side effects studies were conducted on healthy rats to measure the hypoglycemia risk of G-MSN@Insulin@ZnO-PBA-2. Briefly, healthy rats were divided into 2 groups and subcutaneously injected with G-MSN@Insulin@ZnO-PBA-2 (20.5 IU/kg) and insulin (20.5 IU/kg), respectively. BGLs were tested every 30 min over 5 h.

To further evaluate whether the G-MSN@Insulin@ZnO-PBA-2 damage major organs, histopathological analysis was conducted on type 1 diabetic rats. Rats were grouped into 3 groups and subcutaneously injected with PBS, G-MSN@Insulin@ZnO-PBA-2 (20.5 IU/kg) and insulin (20.5 IU/kg) daily for 4 weeks. After 4 weeks, all rats were sacrificed and main organs were harvested for hematoxylin and eosin (H&E) staining.

2.9. Fabrication of nanoparticle-loaded microneedle patches

Microneedle patches were prepared on PDMS mold using micro-mold casting method according to the previous literature [49]. For SGRM patches containing G-MSN@Insulin@ZnO-PBA-2, the casting materials were first prepared by dispersing G-MSN@Insulin@ZnO-PBA-2 into hyaluronic-acid solution (0.5 g/mL). Casting materials (30.0 μL) were added to the surface of the mold and centrifuged under 4390 × g for 10 min, followed by the addition of pure hyaluronic-acid solution (1.0 g/mL) and centrifugated to serve as the backing layer. After desiccation, the SGRM patches were carefully detached from the mold.

For patches containing G-MSN@FITC-Insulin@ZnO-PBA-2, the casting materials were first prepared by dispersing G-MSN@FITC-Insulin@ZnO-PBA-2 into hyaluronic-acid solution (0.5 g/mL). Casting materials (30.0 μL) were added to the surface of the mold and centrifuged under 4390 × g for 10 min, followed by the addition of pure hyaluronic-acid solution (1.0 g/mL) and centrifugated to serve as the backing layer. After desiccation, the microneedle patches were carefully detached from the mold.

For blank patches, the casting materials were pure hyaluronic-acid solution (0.5 g/mL). Casting materials (30.0 μL) were added to the surface of the mold and centrifuged under 4390 × g for 10 min, followed by the addition of pure hyaluronic-acid solution (1.0 g/mL) and centrifugated to serve as the backing layer. After desiccation, the blank patches were carefully detached from the mold.

2.10. Mechanical strength test

The mechanical strength of the microneedle patch was evaluated using a universal static testing system. The force–displacement curves were obtained by putting different microneedle patch (blank patch and SGRM patch containing G-MSN@Insulin@ZnO-PBA-2) against a stainless-steel plate. The initial gauge was set at 1.5 mm between the microneedle patch and the stainless-steel plate. The speed of the plate movement to the patch was set at 0.5 mm s^{-1}. The failure force was recorded as the needles began to buckle[50].

2.11. Skin penetration efficiency test

The prepared microneedle patches (G-MSN@FITC-Insulin@ZnO-PBA-2) were pressed into porcine skin with a thumb. All the needles were completely dissolved after 5 min. To visualize the permeation depth of the microneedle patch, puncture sites of the porcine skin were imaged and recorded by optical microscope and confocal laser scanning microscopy.

2.12. In vivo studies on mice

Type 1 diabetic mice models were induced by STZ intraperitoneal injection. STZ dosage was set at 180.0 mg/kg for mice. Mice were shaved and grouped, including blank patch group, SGRM patch containing G-MSN@Insulin@ZnO-PBA-2 (12.0 IU/kg) group and insulin injection group (12.0 IU/kg). The BGLs were tested over time until they returned to high levels. At the meantime, blood samples were drawn at set times to examine the serum insulin concentration by ELISA kit (MEXN-M0052, China).

IPGTTs were conducted to evaluate the *in vivo* glucose response of the SGRM patches. Briefly, diabetic mice were divided into 2 groups. Two groups were administrated with SGRM patches containing G-MSN@Insulin@ZnO-PBA-2 (12.0 IU/kg) and insulin (12.0 IU/kg). Healthy mice were used as control. After 3 h, mice were intraperitoneally injected with glucose solution (1.5 g/kg). BGLs were tested every 10 min for 2 h. The glucose area under the curve (AUC) between 0 and 120 min was calculated to assess the responsiveness of the SGRM patch towards blood glucose, in comparison with the other groups.

Side effects study was conducted on healthy mice to measure the hypoglycemia risk of SGRM patch. Briefly, healthy mice were divided into 2 groups, including SGRM patch containing G-MSN@Insulin@ZnO-PBA-2 (12.0 IU/kg) and insulin (12.0 IU/kg) as a positive control. BGLs were tested every 30 min over 5 h.

The pharmacodynamic study was conducted on both diabetic and healthy mice. Briefly, diabetic mice were divided into 4 groups, including subcutaneous injection of insulin (12.0 IU/kg), applying SGRM patches containing G-MSN@Insulin@ZnO-PBA-2 (12.0 IU/kg), diabetic mice with no administration and healthy mice as the control group. The daily treatments lasted for 4 weeks and all mice were weighted and tested for BGLs every 3 days. All mice were sacrificed for serological parameter analysis and harvesting of the injection sites for H&E staining and TUNEL staining.

3. Results and discussion

3.1. Preparation and characterization of G-MSN@Insulin@ZnO-PBA-1 and G-MSN@Insulin@ZnO-PBA-2

Mesoporous silica nanoparticle (MSN) and zinc oxide dot (ZnO) were synthesized according to the previous literature [47]. To further functionalize these nanoparticles, gluconamide and PBAs were grafted respectively to obtain G-MSN and ZnO-PBA. The insulin delivery system G-MSN@Insulin@ZnO-PBA was constructed by utilizing dynamic covalent bonds formed between the gluconamide and PBAs. G-MSN was characterized using transmission electron microscopy (TEM) and scanning electron microscopy (SEM) (Fig. 1A; Fig. S8). G-MSN displayed uniform spherical structure (100–120 nm) and orderly-arranged channels. The surface functionalization of MSN was confirmed by Fourier Transform-Infrared Spectroscopy (FT-IR) (Fig. 1D). MSN and G-MSN^0 without template removal showed typical C—H stretching vibrations of CTAB at 2850 cm^{-1} and 2920 cm^{-1}, and C—H bending vibrations at 1475 cm^{-1}. However, the FT-IR of G-MSN showed that these vibrations almost disappeared, indicating the successful removal of CTAB. Enhanced peaks around 1585 cm^{-1} and 1640 cm^{-1} were attributed to the C=O stretching vibrations generated by gluconamide, indicating the successful surface functionalization. ZnO was characterized as uniform spheres (5–10 nm) using TEM (Fig. 1B). The functionalization of ZnO was confirmed by FT-IR, showing that PBAs were successfully grafted onto ZnO to obtain ZnO-PBA-1 and ZnO-PBA-2(Fig. 1E). Insulin was loaded in the pores of G-MSN in PBS solution (pH = 2). After the removal of the supernatant, grafted ZnO was added to block the nanopores. As seen from the TEM images (Fig. 1C), the assembled nanoparticles maintained spherical structures, and the surfaces were covered with small spherical dots, showing that the nano zinc oxides were successfully connected to the surface of the mesoporous silica nanoparticles by a dynamic covalent bond between the gluconamide and PBAs in order to block the insulin from premature release while circulating *in vivo*. The N_2 absorption – desorption measurements (Fig. 1F) further confirmed successful insulin loading and ZnO capping. There were differences in specific surface area, pore size and pore volume of G-MSN, G-MSN@Insulin, G-MSN@Insulin@ZnO-PBA-1 and G-MSN@Insulin@ZnO-PBA-2 (Fig. S9). G-MSN has larger pore size (5.6 nm) and pore volume. After loading insulin, the pore volume and the surface area were significantly reduced, showing that the insulin had been efficiently loaded into the pores. Then, after capping with ZnO-PBA, the specific surface area was further reduced, indicating the successful plugging of the pores by ZnO-PBA. The loading capacity and loading efficiency of G-MSN@Insulin@ZnO-PBA-2 were calculated to be 7.19% and 31.25%, respectively (Fig. S11).

3.2. In vitro glucose response of constructed nanoparticles

The detection of D-glucose by PBAs based fluorescent probes has been investigated intensively over the past three decades [27], however as far as we are aware no previous research has used them as part of an insulin delivery system. The detection limits of some of these molecular probes are at millimolar levels, which is the same as biological glucose levels, as such we considered that they could be used to construct an insulin delivery system. Two promising probes, developed by the James group [51,52], were used to construct G-MSN@Insulin@ZnO-PBA-1 and G-MSN@Insulin@ZnO-PBA-2. In order to compare the response profile of the two constructed nanoparticles, insulin release tests were conducted in PBS (pH = 7.4) solutions with different glucose concentrations, 0 mg/dL, 180 mg/dL, 450 mg/dL, 900 mg/dL. The release profiles of the two nanoparticles all displayed glucose dependent behavior (Fig. 2A and 2B), and the release of FITC-insulin from the nanoparticles corelated with the glucose concentration, which was due to the dynamic covalent binding between PBA and gluconamide being broken by competitive interaction with glucose. G-MSN@FITC-Insulin@ZnO-PBA-2 (Fig. 2B) displayed enhanced sensitivity towards glucose than G-MSN@FITC-Insulin@ZnO-PBA-1, resulting in a 19% release towards 180 mg/dL glucose, mainly because the linker PBA-2 had a higher glucose binding constant (log K = 1.8) and a lower pKa (pKa = 2.9), allowing for competitive binding between glucose and PBA-2 at 180 mg/dL, resulting in facile removal of the "gate-keeper". When the glucose concentration increased gradually from 180, 450 to 900 mg/dL, as shown in Fig. 2C, G-MSN@FITC-Insulin@ZnO-PBA-2 represented sensitive FITC-insulin release property. The pulsatile release profile (Fig. 2D) showed that after first cycle of glucose concentration change, G-MSN@FITC-Insulin@ZnO-PBA-2 remained steady insulin release for the following two rounds. For G-MSN@Insulin@ZnO-PBA-2, the far-UV circular dichroism (CD) spectra at 208 nm suggested that the released insulin retained α-helical secondary structure and bioactivity, compared with the native insulin solution (Fig. S12). Therefore, we utilized G-MSN@Insulin@ZnO-PBA-2 to conduct the *in vivo* experiments on diabetic animal models.

3.3. In vivo studies of G-MSN@Insulin@ZnO-PBA-2 on type 1 diabetic rats

In order to evaluate the diabetic treatment effect of the constructed nanoparticles, STZ-induced type 1 diabetic rats were grouped and subcutaneously injected with PBS, insulin, and G-MSN@Insulin@ZnO-PBA-2, respectively. As shown in Fig. 3A, the

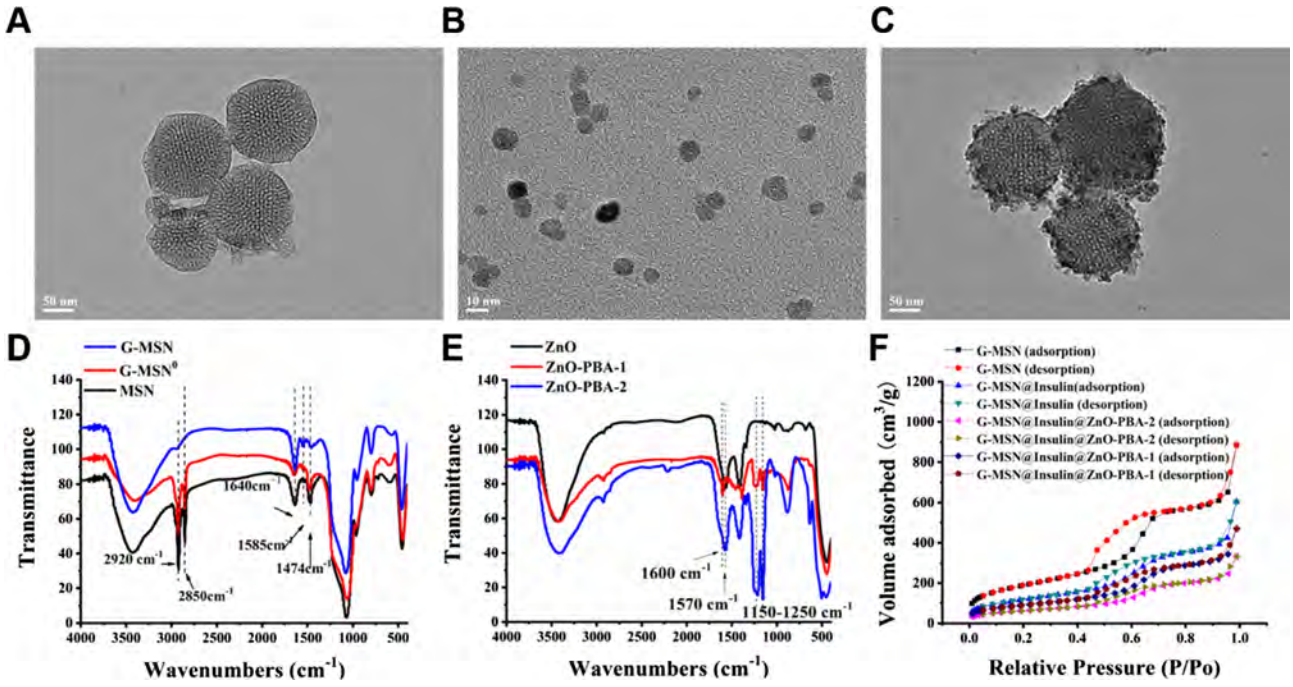

Fig. 1. Characterization of nanoparticles. (**A-C**) TEM images of G-MSN (A), ZnO (B), and G-MSN@Insulin@ZnO-PBA (C). (**D**) Fourier transform infrared (FT-IR) spectroscopy of MSN, G-MSN^0, G-MSN. (**E**) Fourier transform infrared (FT-IR) spectroscopy of ZnO, ZnO-PBA-1, ZnO-PBA-2. (**F**) Nitrogen adsorption – desorption isotherms of G-MSN, G-MSN@Insulin, G-MSN@Insulin@ZnO-PBA-1 and G-MSN@Insulin@ZnO-PBA-2.

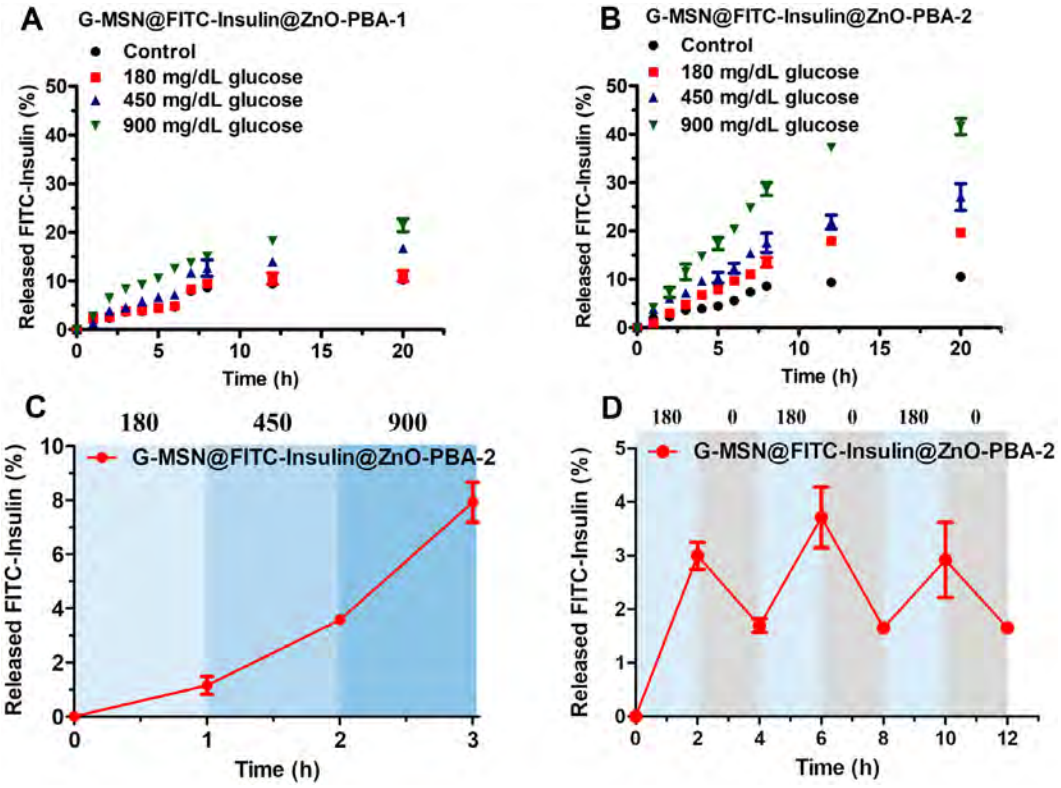

Fig. 2. *In vitro* glucose response of nanoparticles. (**A**) Accumulated insulin release from G-MSN@FITC-Insulin@ZnO-PBA-1 with different glucose concentrations (n = 3). (**B**) Accumulated insulin release from G-MSN@FITC-Insulin@ZnO-PBA-2 with different glucose concentrations (n = 3). (**C**) The release rate (line slope) of G-MSN@FITC-Insulin@ZnO-PBA-2 at 180, 450, 900 mg/dL glucose concentrations (n = 3). (**D**) The pulsatile release profile of G-MSN@FITC-Insulin@ZnO-PBA-2 at 0, 180 mg/dL glucose concentration (n = 3). All experiments were conducted under PBS (pH = 7.4) at 37 °C. Data points represent mean ± SEM.

PBS-treated group remained high BGLs throughout the observation period, indicating the successful establishment of diabetic model. For diabetic rats injected with G-MSN@Insulin@ZnO-PBA-2 (20.5 IU/kg), the BGLs of rats decreased to normal range[17,53] (70–200 mg/dL) in 2 h and remained at a normoglycemic level for about 8 h without occurring hypoglycemia (Fig. 3A), which

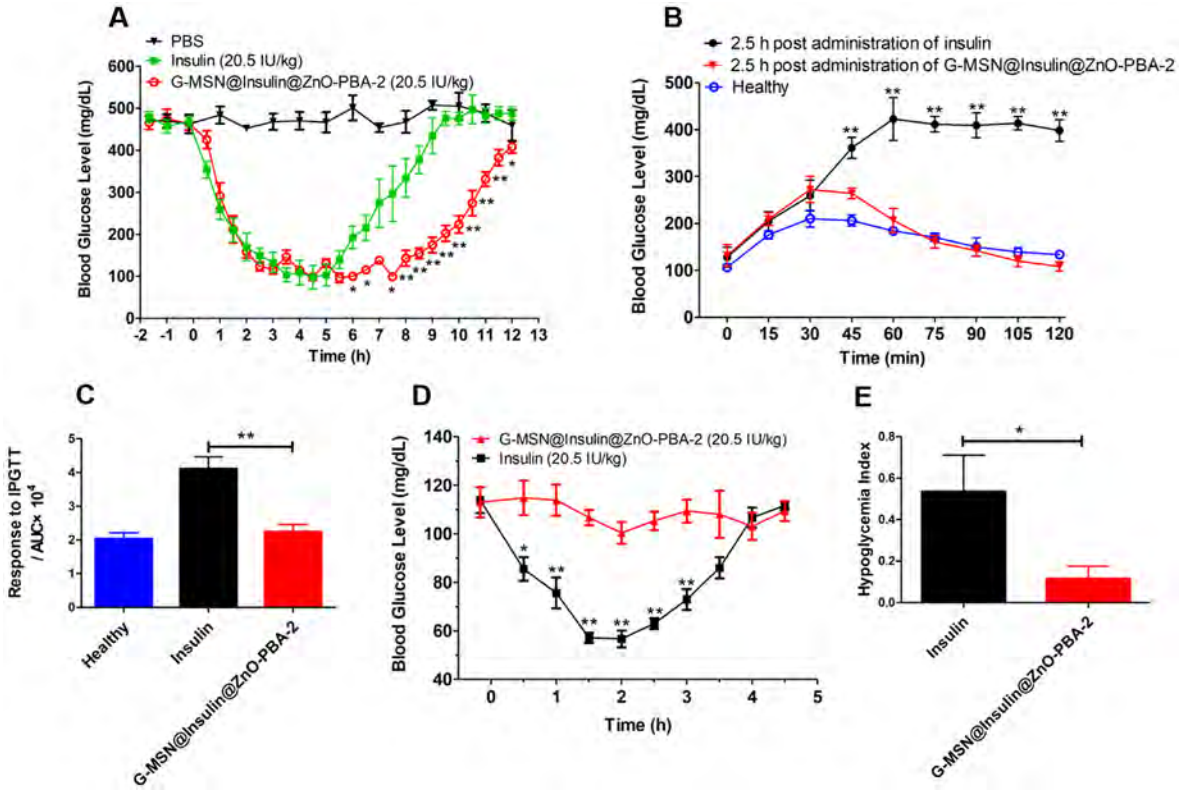

Fig. 3. In vivo studies of G-MSN@Insulin@ZnO-PBA-2 on type 1 diabetic rats. (A) Fasting blood glucose levels of type 1 diabetic rats treated with PBS, insulin (20.5 IU/kg) and G-MSN@Insulin@ZnO-PBA-2 (20.5 IU/kg); $^{**}p < 0.01$, $^{*}p < 0.05$ vs. insulin (20.5 IU/kg), (n = 4). (B) In vivo glucose tolerance test toward diabetic rats 2.5 h post administration of insulin or G-MSN@Insulin@ZnO-PBA-2 (20.5 IU/kg) in comparison to healthy rats; $^{**}p < 0.01$, $^{*}p < 0.05$ vs. healthy rats, (n = 4). (C) Response was calculated according to the area under the curve (AUC) in 120 min, (n = 4). (D) Blood glucose changes of healthy mice treated with G-MSN@Insulin@ZnO-PBA-2 and insulin, (n = 4). (E) Hypoglycemia index was calculated according to the difference between the initial and nadir blood glucose readings divided by the time at which nadir was reached, (n = 4). Student's *t* test was used. Data points represent mean ± SEM.

showed better performance than G-MSN@Insulin@ZnO-PBA-1 (Fig. S13). While, the BGLs of diabetic rats treated with insulin (20.5 IU/kg) quickly decreased to normal range and could only remained stable for<4.5 h.

IPGTTs were conducted 2.5 h after subcutaneous injection of G-MSN@Insulin@ZnO-PBA-2 and insulin (20.5 IU/kg). Healthy rats were treated as the control group without subcutaneous injection. All groups showed quick rises of BGLs after intraperitoneal injection of glucose (1.5 g/kg). The BGLs of diabetic rats treated with insulin alone quickly increased to 400 mg/dL within 60 min and maintained at hyperglycemia state in the following time. While the healthy group and T1D group treated with G-MSN@Insulin@ZnO-PBA-2 showed a decline of BGLs after reaching 260 mg/dL and 200 mg/dL at 30 min, respectively. Then the BGLs of these two groups gradually returned to normoglycemia levels and stayed in the following time (Fig. 3B). To further quantify the glucose responsiveness of G-MSN@Insulin@ZnO-PBA-2, the AUC was calculated from 0 to 120 min. When considering the AUC data, the parameter was significantly lower in G-MSN@Insulin@ZnO-PBA-2 group than insulin alone (Fig. 3C).

In order to verify the risk of hypoglycemia, healthy rats were grouped and subcutaneously injected with insulin and G-MSN@Insulin@ZnO-PBA-2, respectively. The BGLs of healthy rats treated with insulin alone quickly decreased to 60 mg/dL within 1.5 h (Fig. 3D), which indicated the hypoglycemic risk of insulin. While the G-MSN@Insulin@ZnO-PBA-2 group maintained BGLs at normal range without obvious hypoglycemia. Moreover, the administration of insulin alone showed three times risk of hypoglycemia, compared with G-MSN@Insulin@ZnO-PBA-2 group (Fig. 3E).

Furthermore, main organs of diabetic rats were evaluated by H&E staining to assess the potential risk of injected G-MSN@Insulin@ZnO-PBA-2 nanoparticles (Fig. S14). After 4 weeks of treatment, no visible lesions could be observed in the sections of liver, spleen, kidney, heart and lung, which demonstrated that the G-MSN@Insulin@ZnO-PBA-2 nanoparticles didn't cause any obvious damage to the main organs of diabetic rats.

3.4. Fabrication and characterization of microneedle patches

According to the *in vitro* insulin release result and *in vivo* response to glucose, we further used G-MSN@Insulin@ZnO-PBA-2 to conduct consecutive experiments. In order to facilitate facile administration of the nanoparticles, we fabricated hyaluronic-acid based microneedle patches, in which G-MSN@Insulin@ZnO-PBA-2 or G-MSN@FITC-Insulin@ZnO-PBA-2 were loaded according to method described above. As shown in Fig. 4A, the prepared microneedle patches consist of 15 × 15 pyramidal needles, with an approximate height of 500 μm, which is sufficiently long to penetrate the dermis in order to achieve efficient insulin delivery.

The distribution of G-MSN@FITC-Insulin@ZnO-PBA-2 in the microneedle patch was observed by confocal microscope. The nanoparticles were distributed evenly in the upper region of the needles (Fig. 4B and Fig. 4C), while almost no green fluorescence was observed near the base, indicating the successful loading of the nanoparticles, which was essential for efficient transdermal delivery of insulin.

The mechanical strength of the microneedle patches was evaluated using a universal static testing system. Different microneedle patches (blank patch and SGRM patch containing G-

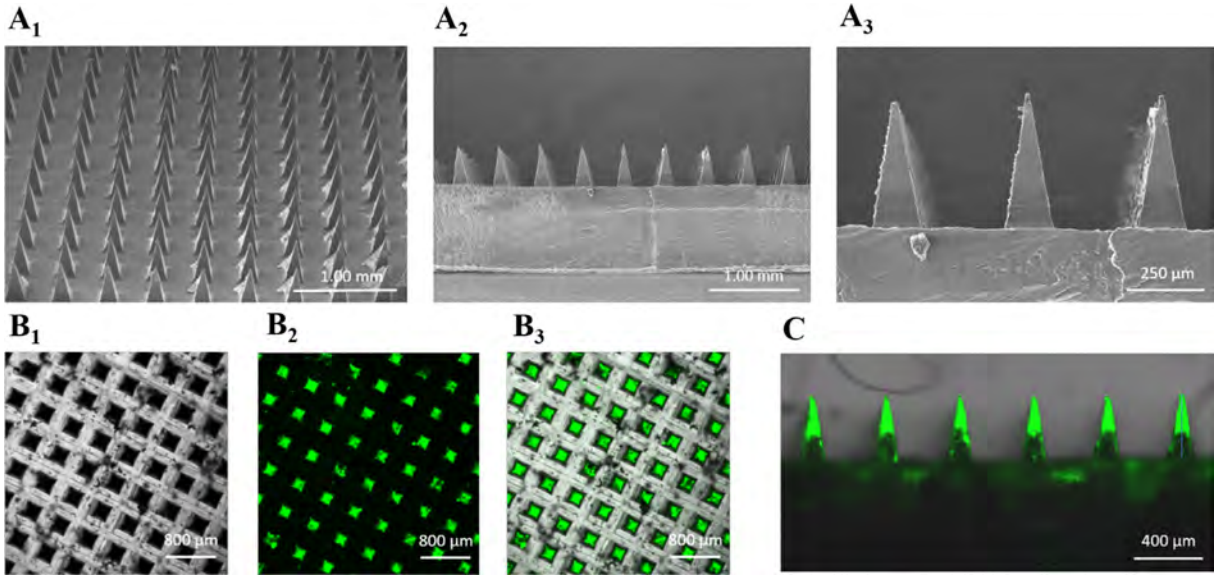

Fig. 4. Characterization of G-MSN@FITC-Insulin@ZnO-PBA-2 loaded microneedle patch. (**A$_1$**, **A$_2$**, and **A$_3$**) SEM image of the microneedle patch. (**B$_1$**, **B$_2$**, and **B$_3$**) Confocal fluorescence microscopy images of the microneedle patch containing G-MSN@FITC-Insulin@ZnO-PBA-2 (**B$_1$**: Bright field; **B$_2$**: FITC green fluorescence image; **B$_3$**: Merged field). (**C**) Fluorescence microscopy image of the microneedle patch containing G-MSN@FITC-Insulin@ZnO-PBA-2.

MSN@Insulin@ZnO-PBA-2 were evaluated to assess the failure force (Fig. S15)[43]. The failure force was 27.96 N for the blank patch and 30.67 N for the SGRM patch when the displacement reached 0.4 mm, which implied sufficient strength and stiffness for efficient skin penetration.

The skin insertion test was conducted using porcine skin to evaluate the transdermal delivery capacity of the microneedle patch (Fig. S16). As shown in Fig. S16A, the porcine skin was smooth before patch treatment. After application for 5 min, the skin displayed ordered tiny holes, which were caused by the patch needles. Then, the same skin was examined under confocal fluorescence microscopy (Fig. S16B). The orderly-arranged cube-like channels revealed that the FITC-insulin was successfully inserted into the skin and retained. All these results indicated that the patch treatment could successfully deliver insulin into the dermis of the skin.

3.5. In vivo studies of SGRM patches on type 1 diabetic mice

To assess the *in vivo* effect of SGRM patches, the STZ-induced type 1 diabetic mice were grouped and treated with different samples, including blank patches containing only HA, insulin and SGRM patches containing G-MSN@Insulin@ZnO-PBA-2. The insulin dosage of each group was set at 12.0 IU/kg.

As shown in Fig. 5A, the BGLs of diabetic mice treated with SGRM patches gradually returned to normal range within 3 h and maintained below 200 mg/dL for about 4.5 h without entering hypoglycemia. While, the BGLs of diabetes mice treated with insulin decreased to about 200 mg/dL in 3 h and maintained for about 1 h, and after that gradually returned to hyperglycemic levels. Thus, SGRM patches treated mice showed 3.5 h longer time of blood glucose regulation than insulin treated only. However, negligible decrease in glucose level was observed in the mice treated with blank patches (HA). As shown in Fig. 5B, after the administration, the serum insulin levels in mice treated with SGRM patches increased to a peak value in 2 h, and then kept a prolonged higher level than those of treated with insulin alone.

IPGTTs were conducted at 3 h after treatment with SGRM patches or insulin, and compared with healthy control group. As shown in Fig. 5C, all groups displayed quick rises in BGLs after intraperitoneal injection of glucose (1.5 g/kg), and the BGLs of mice treated with insulin alone quickly reached 400 mg/dL within 30 min and maintained at the hyperglycemia state in the following 90 min. In contrast, the mice treated with SGRM patches quickly recovered to normoglycemic levels in 30 min and stayed in the following time which is similar to the healthy mice. When AUC from 0 to 120 min was calculated, there was a significant decrease in SGRM patch group in comparison with insulin alone (Fig. 5D).

In order to assess the risk of hypoglycemia, healthy mice were grouped and administrated with insulin alone and SGRM patches, respectively (Fig. 5E and Fig. 5F). The BGLs of mice treated with insulin alone quickly showed hypoglycemia in 1.5 h, about 55 mg/dL. While, no significant decrease in BGLs was observed in SGRM patches treated mice. Moreover, the administration of SGRM patches alleviated the risk of hypoglycemia, compared with insulin group (Fig. 5F).

Four weeks therapy was further conducted to verify the efficacy of the SGRM patches treatment and the biosafety of SGRM patches towards the skin (Fig. S17). Glycosylated hemoglobin (GHb) was tested to monitor the long-term BGLs control of diabetic mice. The results indicated that mice treated with SGRM patches daily for four weeks exhibited similar GHb concentrations to healthy mice, which meant that the SGRM patch treatment was more efficient in controlling the BGLs of diabetic mice when compared with the group treated with insulin only. In addition, total cholesterol (TC) and triglyceride (TG) in the serum was also attenuated in the SGRM patches treated group when compared to the insulin group, which further indicated the efficacy of the SGRM patches treatment. Furthermore, the biomarker of liver damage, including alanine aminotransferase (ALT), aspartate transaminase (AST), serum albumin (Alb), and total protein (TP), as well as the biomarker of renal function, blood urea nitrogen (BUN), were also improved. These results indicated that the liver and renal function of diabetic mice treated with the SGRM patches were better protected, compared with the insulin treated group.

What's more, SGRM patches treatment also had enhancement on mice BGLs and body weight (measured every 3 days), compared with insulin treatment alone (Fig. S18 and Fig. S19). Finally, H&E staining (Fig. S20) and TUNEL assay (Fig. S21) were conducted to intuitively analyze the biocompatibility of SGRM patches towards

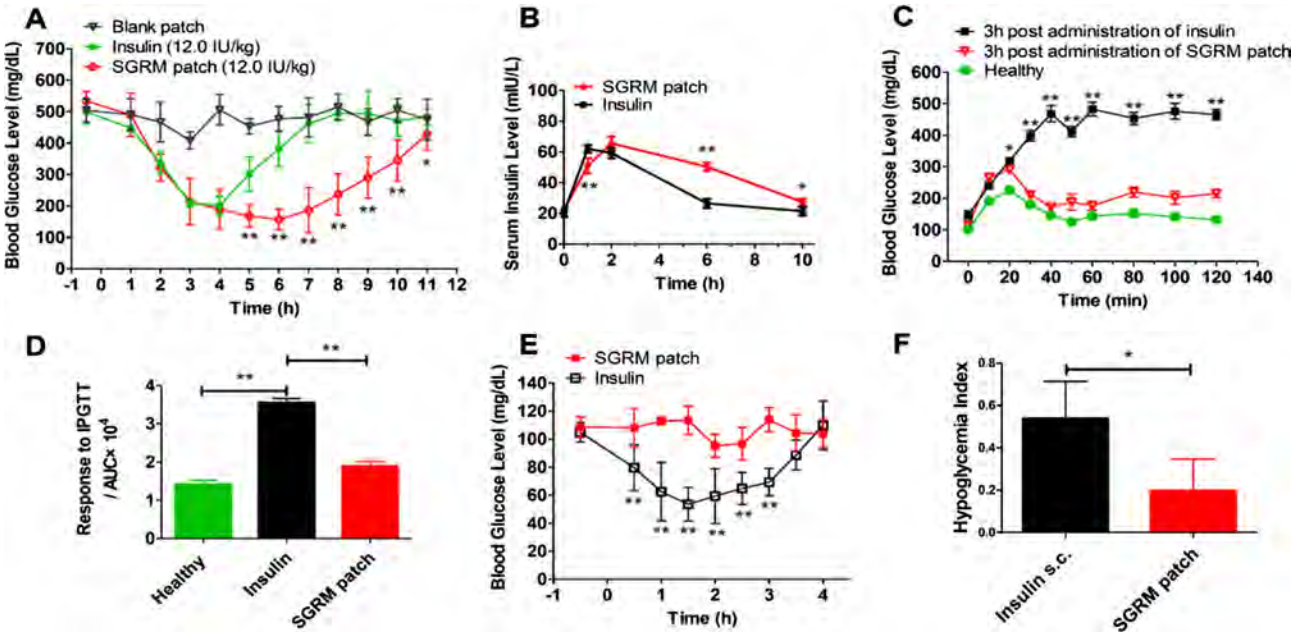

Fig. 5. In vivo studies of SGRM patches on type 1 diabetic mice. (**A**) Blood glucose levels of type 1 diabetic mice treated with blank patches, insulin (12.0 IU/kg) and SGRM patches (12.0 IU/kg); $^{**}P < 0.01$, $^{*}P < 0.05$ vs. insulin (12.0 IU/kg), (n = 4). (**B**) Insulin concentration − time curves of diabetic mice treated with SGRM patches and insulin, (n = 4). (**C**) In vivo glucose tolerance test of diabetic mice 3 h post administration of insulin or SGRM patches in comparison to healthy mice; $^{**}P < 0.01$, $^{*}P < 0.05$ vs. healthy mice, (n = 4). (**D**) Response was calculated according to the area under the curve (AUC) over 120 min, (n = 4). (**E**) Blood glucose changes of healthy mice treated with SGRM patches and insulin, (n = 4). (**F**) Hypoglycemia index was calculated according to the difference between the initial and nadir blood glucose readings divided by the time at which nadir was reached, (n = 4). Student's *t* test was used. Data points represent mean ± SEM.

skins, which showed that both SGRM patches treated group and the insulin treated group displayed no significant tissue rupture and inflammation.

4. Conclusions

We have successfully constructed an insulin delivery system G-MSN@Insulin@ZnO-PBA-2 for type 1 diabetic treatments. Wulff-type phenylboronic acid was firstly used as the glucose responsive linker in an insulin delivery system, achieving both prolonged BGLs regulation and avoided of hypoglycemia *in vivo* compared with other PBAs based insulin delivery systems [30,31,33–37]. The unique Wulff-type phenylboronic acid PBA-2 on ZnO-PBA-2 could forms stable boronic ester with diols on G-MSN under physiological condition, while the boronic ester was completely broken under high BGLs, thus the capping agent was detached from G-MSN and insulin was released from the pores. Furthermore, G-MSN@Insulin@ZnO-PBA-2 was incorporated into hyaluronic-acid based dissolving microneedle patch to reduce the pain of injection and achieve convenient administration, which could result in the development of desirable smart insulin delivery system with the potential for clinical application. Further studies would focus on the long-term biosafety and biodistribution of G-MSN@Insulin@ZnO-PBA-2.

CRediT authorship contribution statement

Yun Fu: Conceptualization, Investigation, Writing – original draft. **Peng Liu:** Investigation, Writing – original draft. **Meng Chen:** Validation. **Tongxia Jin:** Investigation. **Huijing Wu:** Investigation. **Mingyang Hei:** Conceptualization. **Congrong Wang:** Supervision, Writing - review & editing. **Yufang Xu:** Supervision. **Xuhong Qian:** Supervision. **Weiping Zhu:** Conceptualization, Supervision, Writing - review & editing.

Declaration of Competing Interest

The authors declare that they have no known competing financial interests or personal relationships that could have appeared to influence the work reported in this paper.

Acknowledgement

This work was supported by National Natural Science Foundation of China(Grants 21878088, 21476077, 82070913), Key projects of Shanghai Science and Technology Commission (18DZ1112703), Shanghai Science and Technology Development Funds(20ZR1446000) and Research start-up fund from Shanghai Fourth People's Hospital(sykyqd01801).

Appendix A. Supplementary material

Supplementary data to this article can be found online at https://doi.org/10.1016/j.jcis.2021.07.126.

References

[1] S. Genuth, K.G.M.M. Alberti, P. Bennett, J. Buse, R. DeFronzo, R. Kahn, J. Kitzmiller, W.C. Knowler, H. Lebovitz, A. Lernmark, D. Nathan, J. Palmer, R. Rizza, C. Saudek, J. Shaw, M. Steffes, M. Stern, J. Tuomilehto, P. Zimmet, E.C.D. Classificat, Follow-up report on the diagnosis of diabetes mellitus, Diabetes Care 26 (11) (2003) 3160–3167.

[2] M. Stumvoll, B.J. Goldstein, T.W. van Haeften, Type 2 diabetes: pathogenesis and treatment, Lancet 371 (9631) (2008) 2153–2156.

[3] P. Saeedi, I. Petersohn, P. Salpea, B. Malanda, S. Karuranga, N. Unwin, S. Colagiuri, L. Guariguata, A.A. Motala, K. Ogurtsova, J.E. Shaw, D. Bright, R. Williams, R. Almutairi, P.A. Montoya, A. Basit, S. Besanccon, C. Bommer, W. Borgnakke, E. Boyko, J.L. Chan, H. Divakar, A. Esteghamati, N. Forouhi, L. Franco, E. Gregg, M. Hassanein, C. Ke, D. Levitt, L.L. Lim, G.D. Ogle, D. Owens, M. Pavkov, J. Pearson-Stuttard, A. Ramachandran, W. Rathmann, M. Riaz, D. Simmons, A. Sinclair, E. Sobngwi, R. Thomas, H. Ward, S. Wild, X.L. Yang, L.L. Yuen, P. Zhang, I.D.A. Comm, Global and regional diabetes prevalence estimates for 2019 and projections for 2030 and 2045: Results from the International Diabetes Federation Diabetes Atlas, 9th edition, Diabetes Res Clin Pr 157 (2019) 107843.

[4] J.B. Halter, N. Musi, F.M. Horne, J.P. Crandall, A. Goldberg, L. Harkless, W.R. Hazzard, E.S. Huang, M.S. Kirkman, J. Plutzky, K.E. Schmader, S. Zieman, K.P. High, Diabetes and Cardiovascular Disease in Older Adults: Current Status and Future Directions, Diabetes 63 (8) (2014) 2578–2589.
[5] S.G. Frodsham, Z. Yu, A.M. Lyons, A. Agarwal, M.H. Pezzolesi, L.i. Dong, T.R. Srinivas, J. Ying, T. Greene, K.L. Raphael, K.R. Smith, M.G. Pezzolesi, The Familiality of Rapid Renal Decline in Diabetes, Diabetes 68 (2) (2019) 420–429.
[6] R. van Crevel, S. van de Vijver, D.A.J. Moore, The global diabetes epidemic: what does it mean for infectious diseases in tropical countries?, Lancet Diabetes Endo 5 (6) (2017) 457–468
[7] X.Y. Li, X. Qi, G.H. Yuan, S. Ju, Z.Y. Yu, W. Deng, Y.J. Liu, Y.F. Li, X.J. Bu, M.C. Ding, Q. Li, X.H. Guo, Microbiological profile and clinical characteristics of diabetic foot infection in northern China: a retrospective multicentre survey in the Beijing area, J Med Microbiol 67 (2) (2018) 160–168.
[8] G. Scheiner, R.J. Sobel, D.E. Smith, A.J. Pick, D. Kruger, J. King, K. Green, Insulin Pump Therapy Guidelines for Successful Outcomes, Diabetes Educator 35 (2009) 29s–41s.
[9] R. Mo, T.Y. Jiang, J. Di, W.Y. Tai, Z. Gu, Emerging micro-and nanotechnology based synthetic approaches for insulin delivery, Chem Soc Rev 43 (10) (2014) 3595–3629.
[10] J. Yu, Y. Zhang, Y. Ye, R. DiSanto, W. Sun, D. Ranson, F.S. Ligler, J.B. Buse, Z. Gu, Microneedle-array patches loaded with hypoxia-sensitive vesicles provide fast glucose-responsive insulin delivery, Proceedings of the National Academy of Sciences of the United States of America 112 (27) (2015) 8260–8265.
[11] J. Wang, Y. Ye, J. Yu, A.R. Kahkoska, X. Zhang, C. Wang, W. Sun, R.D. Corder, Z. Chen, S.A. Khan, J.B. Buse, Z. Gu, Core-Shell Microneedle Gel for Self-Regulated Insulin Delivery, Acs Nano 12 (3) (2018) 2466–2473.
[12] R. Yin, K. Wang, S. Du, L.u. Chen, J. Nie, W. Zhang, Design of genipin-crosslinked microgels from concanavalin A and glucosyloxyethyl acrylated chitosan for glucose-responsive insulin delivery, Carbohyd Polym 103 (2014) 369–376.
[13] Y. Xiao, H. Sun, J. Du, Sugar-Breathing Glycopolymersomes for Regulating Glucose Level, J Am Chem Soc 139 (22) (2017) 7640–7647.
[14] L. Hou, Y. Zheng, Y. Wang, Y. Hu, J. Shi, Q.i. Liu, H. Zhang, Z. Zhang, Self-Regulated Carboxyphenylboronic Acid-Modified Mesoporous Silica Nanoparticles with "Touch Switch" Releasing Property for Insulin Delivery, Acs Appl Mater Inter 10 (26) (2018) 21927–21938.
[15] H. Yang, R. Ma, J. Yue, C. Li, Y. Liu, Y. An, L. Shi, A facile strategy to fabricate glucose-responsive vesicles via a template of thermo-sensitive micelles, Polym Chem-Uk 6 (20) (2015) 3837–3846.
[16] Z. Gu, T.T. Dang, M.L. Ma, B.C. Tang, H. Cheng, S. Jiang, Y.Z. Dong, Y.L. Zhang, D. G. Anderson, Glucose-Responsive Microgels Integrated with Enzyme Nanocapsules for Closed-Loop Insulin Delivery, Acs Nano 7 (8) (2013) 6758–6766.
[17] X.L. Hu, J.C. Yu, C.G. Qian, Y. Lu, A.R. Kahkoska, Z.G. Xie, X.B. Jing, J.B. Buse, Z. Gu, H2O2-Responsive Vesicles Integrated with Transcutaneous Patches for Glucose-Mediated Insulin Delivery, Acs Nano 11 (1) (2017) 613–620.
[18] J.C. Yu, C.G. Qian, Y.Q. Zhang, Z. Cui, Y. Zhu, Q.D. Shen, F.S. Ligler, J.B. Buse, Z. Gu, Hypoxia and H2O2 Dual-Sensitive Vesicles for Enhanced Glucose-Responsive Insulin Delivery, Nano Lett 17 (2) (2017) 733–739.
[19] M. Oroval, P. Diez, E. Aznar, C. Coll, M.D. Marcos, F. Sancenon, R. Villalonga, R. Martinez-Manez, Self-Regulated Glucose-Sensitive Neoglycoenzyme-Capped Mesoporous Silica Nanoparticles for Insulin Delivery, Chem-Eur J 23 (6) (2017) 1353–1360.
[20] W.H. Chen, G.F. Luo, M. Vazquez-Gonzalez, R. Cazelles, Y.S. Sohn, R. Nechushtai, Y. Mandel, I. Willner, Glucose-Responsive Metal-Organic-Framework Nanoparticles Act as "Smart" Sense-and-Treat Carriers, Acs Nano 12 (8) (2018) 7538–7545.
[21] B. Xu, G.H. Jiang, W.J. Yu, D.P. Liu, Y. Zhang, J.Y. Zhou, S.Q. Sun, Y.K. Liu, H2O2-Responsive mesoporous silica nanoparticles integrated with microneedle patches for the glucose-monitored transdermal delivery of insulin, J Mater Chem B 5 (41) (2017) 8200–8208.
[22] Z. Gu, A.A. Aimetti, Q. Wang, T.T. Dang, Y.L. Zhang, O. Veiseh, H. Cheng, R.S. Langer, D.G. Anderson, Injectable Nano-Network for Glucose-Mediated Insulin Delivery, Acs Nano 7 (5) (2013) 4194–4201.
[23] I. Benzeval, A. Bowyer, J. Hubble, The influence of degree-of-branching and molecular mass on the interaction between dextran and Concanavalin A in hydrogel preparations intended for insulin release, Eur J Pharm Biopharm 80 (1) (2012) 143–148.
[24] M.J. Taylor, R. Gregory, P. Tomlins, D. Jacob, J. Hubble, T.S. Sahota, Closed-loop glycaemic control using an implantable artificial pancreas in diabetic domestic pig (Sus scrofa domesticus), Int J Pharmaceut 500 (1–2) (2016) 371–378.
[25] W.L.A. Brooks, C.C. Deng, B.S. Sumerlin, Structure-Reactivity Relationships in Boronic Acid-Diol Complexation, Acs Omega 3 (12) (2018) 17863–17870.
[26] W.L.A. Brooks, B.S. Sumerlin, Synthesis and Applications of Boronic Acid-Containing Polymers: From Materials to Medicine, Chem Rev 116 (3) (2016) 1375–1397.
[27] X.L. Sun, T.D. James, Glucose Sensing in Supramolecular Chemistry, Chem Rev 115 (15) (2015) 8001–8037.
[28] R.J. Ma, L.Q. Shi, Phenylboronic acid-based glucose-responsive polymeric nanoparticles: synthesis and applications in drug delivery, Polym Chem-Uk 5 (5) (2014) 1503–1518.
[29] Q. Huang, L. Wang, H.J. Yu, K. Ur-Rahman, Advances in phenylboronic acid-based closed-loop smart drug delivery system for diabetic therapy, J Control Release 305 (2019) 50–64.
[30] H. Yang, C. Zhang, C. Li, Y. Liu, Y.L. An, R.J. Ma, L.Q. Shi, Glucose-Responsive Polymer Vesicles Templated by alpha-CD/PEG Inclusion Complex, Biomacromolecules 16 (4) (2015) 1372–1381.
[31] A. Matsumoto, T. Ishii, J. Nishida, H. Matsumoto, K. Kataoka, Y. Miyahara, A Synthetic Approach Toward a Self-Regulated Insulin Delivery System, Angew Chem Int Edit 51 (9) (2012) 2124–2128.
[32] G. Springsteen, B.H. Wang, A detailed examination of boronic acid-diol complexation, Tetrahedron 58 (26) (2002) 5291–5300.
[33] Y.J. Zhang, M.X. Wu, W.B. Dai, Y.P. Li, X. Wang, D. Tan, Z.L. Yang, S. Liu, L.J. Xue, Y.F. Lei, Gold nanoclusters for controlled insulin release and glucose regulation in diabetes, Nanoscale 11 (13) (2019) 6471–6479.
[34] A. Matsumoto, M. Tanaka, H. Matsumoto, K. Ochi, Y. Moro-oka, H. Kuwata, H. Yamada, I. Shirakawa, T. Miyazawa, H. Ishii, K. Kataoka, Y. Ogawa, Y. Miyahara, T. Suganami, Synthetic "smart gel" provides glucose-responsive insulin delivery in diabetic mice, Sci Adv 3 (11) (2017) eaaq0723.
[35] R.J. Ma, H. Yang, Z. Li, G. Liu, X.C. Sun, X.J. Liu, Y.L. An, L.Q. Shi, Phenylboronic Acid-Based Complex Micelles with Enhanced Glucose-Responsiveness at Physiological pH by Complexation with Glycopolymer, Biomacromolecules 13 (10) (2012) 3409–3417.
[36] H.L. Guo, H.M. Li, J.T. Gao, G.X. Zhao, L.L. Ling, B. Wang, Q.Q. Guo, Y. Gu, C.X. Li, Phenylboronic acid-based amphiphilic glycopolymeric nanocarriers for in vivo insulin delivery, Polym Chem-Uk 7 (18) (2016) 3189–3199.
[37] C. Li, X.Y. Liu, Y. Liu, F. Huang, G. Wu, Y. Liu, Z.Z. Zhang, Y.X. Ding, J. Lv, R.J. Ma, Y.L. An, L.Q. Shi, Glucose and H2O2 dual-sensitive nanogels for enhanced glucose-responsive insulin delivery, Nanoscale 11 (18) (2019) 9163–9175.
[38] K.T. Kim, J.J.L.M. Cornelissen, R.J.M. Nolte, J.C.M. van Hest, Polymeric Monosaccharide Receptors Responsive at Neutral pH, J Am Chem Soc 131 (39) (2009) 13908–13909.
[39] S. Badhulika, C. Tlili, A. Mulchandani, Poly(3-aminophenylboronic acid)-functionalized carbon nanotubes-based chemiresistive sensors for detection of sugars, Analyst 139 (12) (2014) 3077–3082.
[40] H.M. Lin, W.K. Wang, P.A. Hsiung, S.G. Shyu, Light-sensitive intelligent drug delivery systems of coumarin-modified mesoporous bioactive glass, Acta Biomater 6 (8) (2010) 3256–3263.
[41] T.D. James, K.R.A.S. Sandanayake, S. Shinkai, Novel Photoinduced Electron-Transfer Sensor for Saccharides Based on the Interaction Of Boronic Acid And Amine, J Chem Soc Chem Comm (4) (1994) 477–478.
[42] J.C. Yu, J.Q. Wang, Y.Q. Zhang, G.J. Chen, W.W. Mao, Y.Q. Ye, A.R. Kahkoska, J.B. Buse, R. Langer, Z. Gu, Glucose-responsive insulin patch for the regulation of blood glucose in mice and minipigs, Nat Biomed Eng 4 (5) (2020) 499–506.
[43] S.Y. Chen, H. Matsumoto, Y. Moro-oka, M. Tanaka, Y. Miyahara, T. Suganami, A. Matsumoto, Microneedle-Array Patch Fabricated with Enzyme-Free Polymeric Components Capable of On-Demand Insulin Delivery, Adv Funct Mater 29 (7) (2019) 1807369.
[44] B.Z. Chen, L.Q. Zhang, Y.Y. Xia, X.P. Zhang, X.D. Guo, A basal-bolus insulin regimen integrated microneedle patch for intraday postprandial glucose control, Sci Adv 6 (28) (2020) eaba7260.
[45] J. Yang, X.L. Liu, Y.Z. Fu, Y.J. Song, Recent advances of microneedles for biomedical applications: drug delivery and beyond, Acta Pharmaceutica Sinica B 9 (3) (2019) 469–483.
[46] C.J. Ward, P. Patel, P.R. Ashton, T.D. James, A molecular colour sensor for monosaccharides, Chem Commun (3) (2000) 229–230.
[47] M.Y. Hei, H.J. Wu, Y. Fu, Y.F. Xu, W.P. Zhu, Phenylboronic acid functionalized silica nanoparticles with enlarged ordered mesopores for efficient insulin loading and controlled release, J Drug Deliv Sci Tec 51 (2019) 320–326.
[48] K.K. Wu, Y. Huan, Streptozotocin-induced diabetic models in mice and rats, Current protocols in pharmacology Chapter 5 (47) (2008) 1–14.
[49] J.W. Lee, J.H. Park, M.R. Prausnitz, Dissolving microneedles for transdermal drug delivery, Biomaterials 29 (13) (2008) 2113–2124.
[50] S.Y. Chen, H. Matsumoto, Y. Moro-oka, M. Tanaka, Y. Miyahara, T. Suganami, A. Matsumoto, Microneedle-Array Patch Fabricated with Enzyme-Free Polymeric Components Capable of On-Demand Insulin Delivery, Adv Funct Mater 29 (7) (2019).
[51] T.D. James, K.R.A.S. Sandanayake, R. Iguchi, S. Shinkai, Novel Saccharide-Photoinduced Electron-Transfer Sensors Based on the Interaction Of Boronic Acid And Amine, J Am Chem Soc 117 (35) (1995) 8982–8987.
[52] C.J. Ward, P. Patel, T.D. James, Boronic acid appended azo dyes-colour sensors for saccharides, J Chem Soc Perk T 1 (4) (2002) 462–470.
[53] A. GhavamiNejad, J. Li, B. Lu, L.W. Zhou, L. Lam, A. Giacca, X.Y. Wu, Glucose-Responsive Composite Microneedle Patch for Hypoglycemia-Triggered Delivery of Native Glucagon, Adv Mater 31 (30) (2019) 1901051.